JACC: CARDIOVASCULAR IMAGING VOL. 17, NO. 2, 2024

PUBLISHED BY ELSEVIER

iREVIEW

STATE-OF-THE-ART REVIEW

Current and Evolving Multimodality Cardiac Imaging in Managing Transthyretin Amyloid Cardiomyopathy

Louhai Alwan, MD,[a] Dominik C. Benz, MD,[b,c,d,e] Sarah A.M. Cuddy, MD,[b,c,d] Stephan Dobner, MD, PhD,[a] Isaac Shiri, PhD,[a] Federico Caobelli, MD,[f] Benedikt Bernhard, MD,[a,d] Simon F. Stämpfli, MD, MS,[g] Franz Eberli, MD,[h] Mauricio Reyes, PhD,[i,j] Raymond Y. Kwong, MD, MPH,[d] Rodney H. Falk, MD,[b] Sharmila Dorbala, MD, MPH,[b,c,d] Christoph Gräni, MD, PhD[a]

ABSTRACT

Amyloid transthyretin (ATTR) amyloidosis is a protein-misfolding disease characterized by fibril accumulation in the extracellular space that can result in local tissue disruption and organ dysfunction. Cardiac involvement drives morbidity and mortality, and the heart is the major organ affected by ATTR amyloidosis. Multimodality cardiac imaging (ie, echocardiography, scintigraphy, and cardiac magnetic resonance) allows accurate diagnosis of ATTR cardiomyopathy (ATTR-CM), and this is of particular importance because ATTR-targeting therapies have become available and probably exert their greatest benefit at earlier disease stages. Apart from establishing the diagnosis, multimodality cardiac imaging may help to better understand pathogenesis, predict prognosis, and monitor treatment response. The aim of this review is to give an update on contemporary and evolving cardiac imaging methods and their role in diagnosing and managing ATTR-CM. Further, an outlook is presented on how artificial intelligence in cardiac imaging may improve future clinical decision making and patient management in the setting of ATTR-CM. (J Am Coll Cardiol Img 2024;17:195–211) © 2024 by the American College of Cardiology Foundation.

Amyloidosis is a group of progressive protein-misfolding diseases characterized by the accumulation of subtype-specific misfolded protein fibrils (amyloid) in the extracellular space. Although amyloidosis is a multiorgan disease and can result in local tissue disruption and dysfunction of several organs in parallel, cardiac involvement (ie, cardiomyopathy [CM]) typically determines the prognosis. More than a dozen amyloid precursor proteins have been identified in patients with cardiac

From the [a]Department of Cardiology, Inselspital, Bern University Hospital, University of Bern, Bern, Switzerland; [b]Amyloidosis Program, Division of Cardiology, Department of Medicine, Brigham and Women's Hospital and Harvard Medical School, Boston, Massachusetts, USA; [c]Division of Nuclear Medicine, Department of Radiology, Brigham and Women's Hospital and Harvard Medical School, Boston, Massachusetts, USA; [d]CV Imaging Program, Cardiovascular Division, Department of Medicine and Radiology, Brigham and Women's Hospital and Harvard Medical School, Boston, Massachusetts, USA; [e]Cardiac Imaging, Department of Cardiology and Nuclear Medicine, Zurich University Hospital, Zurich, Switzerland; [f]University Clinic of Nuclear Medicine, Inselspital, Bern University Hospital, Switzerland; [g]Department of Cardiology, Heart Centre Lucerne, Luzerner Kantonsspital, Lucerne, Switzerland; [h]Department of Cardiology, Triemli Hospital (Triemlispital), Zurich, Switzerland; [i]Insel Data Science Center, Inselspital, Bern University Hospital, Bern, Switzerland; and the [j]Artificial Intelligence in Medical Imaging, ARTORG Center for Biomedical Research, University of Bern, Bern, Switzerland.

Jonathan Weinsaft, MD, served as Guest Editor for this paper.

The authors attest they are in compliance with human studies committees and animal welfare regulations of the authors' institutions and Food and Drug Administration guidelines, including patient consent where appropriate. For more information, visit the Author Center.

Manuscript received August 29, 2023; revised manuscript received October 6, 2023, accepted October 18, 2023.

ISSN 1936-878X/$36.00 https://doi.org/10.1016/j.jcmg.2023.10.010

JACC: CARDIOVASCULAR IMAGING, VOL. 17, NO. 2, 2024
FEBRUARY 2024:195–211

ABBREVIATIONS AND ACRONYMS

AL = amyloid light-chain

ATTR = amyloid transthyretin

DL = deep learning

DPD = 3,3-diphosphono-1,2-propanodicarboxylic acid

EFSR = ratio of ejection fraction to global longitudinal strain

FL = federated learning

H/CL ratio = heart-to-contralateral lung ratio

ML = machine learning

MP = monoclonal protein

PYP = pyrophosphate

RELAPS = ratio of apical longitudinal strain to the sum of base and midlongitudinal strain

SAB = septal apical-to-base longitudinal strain

amyloidosis, yet cases are mostly attributed to amyloid transthyretin (ATTR) and clonal amyloid light-chain (AL) immunoglobulins.[1,2] Among other factors, the awareness and use of additional imaging techniques, rather than relying solely on echocardiography and invasive biopsy, may be contributing factors in the earlier detection of ATTR in recent years.[3-6] Conversely, despite an increase in the detection rate more than the past decade, ATTR-CM probably still remains an underdiagnosed condition.[6] This is reflected by the fact that the diagnosis of ATTR-CM is challenging because clinical, biomarker, and imaging findings often overlap with other those of cardiac conditions. Multimodality cardiac imaging technologies (ie, echocardiography, scintigraphy, and cardiac magnetic resonance [CMR]) not only offer the opportunity for accurate noninvasive diagnostic but may also provide insights into the pathophysiology of ATTR-CM, to better assess individual patient prognosis and help to monitor disease progression and therapeutic efficacy. Therefore, the aims of this review are as follows: 1) to outline the current central role of multimodality cardiac imaging in the management of ATTR-CM; 2) to depict evolving multimodality cardiac imaging methods; and 3) to discuss the future role of artificial intelligence (AI) in this clinical setting.

INTEGRATION OF CARDIAC IMAGING IN CURRENT ATTR-CM RECOMMENDATIONS IN THE EUROPEAN UNION AND THE UNITED STATES

Current diagnostic algorithms by the American Heart Association (AHA),[7] the European Society of Cardiology (ESC),[8] and very recently by the American College of Cardiology (ACC)[9] (**Figure 1**) reflect the "paradigm shift" where noninvasive cardiac imaging and laboratory testing represent the cornerstones in the stepwise evaluation of patients with suspected cardiac amyloidosis. The diagnostic guidelines have a 2-fold aim: 1) to direct clinicians to a diagnosis of cardiac amyloidosis; and 2) if the diagnosis is suspected, to help distinguish between the 2 main types of cardiac amyloidosis—AL amyloidosis (a plasma cell disorder, in which there is almost always an abnormality in circulating monoclonal protein [MP]) and ATTR-CM (in which the precursor protein is either wild-type or variant transthyretin). MP testing in the guidelines consists of measurement of serum and urine protein electrophoresis, serum and urine immunofixation, and serum free light-chain assay.

Step 1: All 3 (ESC, AHA, and ACC) guidelines highlight that in the first step, "red flags" or "clues," in the absence of other heart failure reasons and excluding alternative underlying causes of increased left ventricular (LV) thickness (ie, hypertrophic CM [HCM], hypertensive heart disease, infiltrative cardiomyopathies or aortic stenosis), should prompt consideration of cardiac amyloidosis and trigger further downstream testing. Besides clinical features, electrocardiography (ECG) parameters including low voltage (ie, QRS amplitude ≤5 mm [0.5 mV] in all peripheral leads)[10] and echocardiographic findings such as symmetrical or asymmetrical wall thickening with an inferolateral wall thickness cutoff of ≥14 mm (area under the curve [AUC]: 0.73), average basal longitudinal strain ≥−8% (AUC: 0.76),[11] and a relative apical sparing ratio >1 (AUC: 0.53 [95% CI: 0.52-0.55]),[11,12] should raise the suspicion of ATTR-CM.

Step 2: After initial assessments, diagnostic routes diverge across guidelines. Whereas the ESC suggests a 2-pronged approach consisting of MP testing and bone scintigraphy, the AHA and ACC guidelines focus primarily on the MP assessment and likely reflect improved understanding of the benefit of sequential downstream use of imaging.

Step 3: On the basis of MP results and the Perugini score, the ESC provides the following directives: Although in patients with a negative MP test result with a zero Perugini score the likelihood of ATTR-CM is minimized, a Perugini score of 1 calls for an endomyocardial biopsy, and scores between 2 and 3 confirm ATTR-CM and necessitate genetic testing to distinguish between hereditary and wild-type ATTR amyloidosis. Positive MP findings with a zero Perugini score prompt further CMR imaging, with subsequent biopsy in CMR-positive or inconclusive CMR cases, while ATTR-CM can be ruled out in patients with CMR imaging without any signs of cardiac amyloidosis. When typical CMR findings for amyloidosis align with extracardiac biopsy verification of ATTR in the case of negative MP test results, this pairing is sufficient to establish a diagnosis of ATTR-CM and thus makes scintigraphy unnecessary. According to the AHA and ACC, a positive MP test result directly necessitates a biopsy, thereby bypassing the need for scintigraphy. Conversely, in cases of negative MP test results, decisions are contingent on the Perugini score. If noninvasive imaging is suggestive of cardiac amyloidosis and the Perugini score is 0 to 1, biopsy is suggested, whereas a Perugini score of 2 to 3 demands genetic differentiation from wild-type and hereditary forms, identical to the ESC guidelines. More than 20% of patients with wild-type ATTR-CM have a monoclonal gammopathy of

FIGURE 1 **Comparing Diagnostic Algorithms for Cardiac Amyloidosis (ESC, AHA, and ACC)**

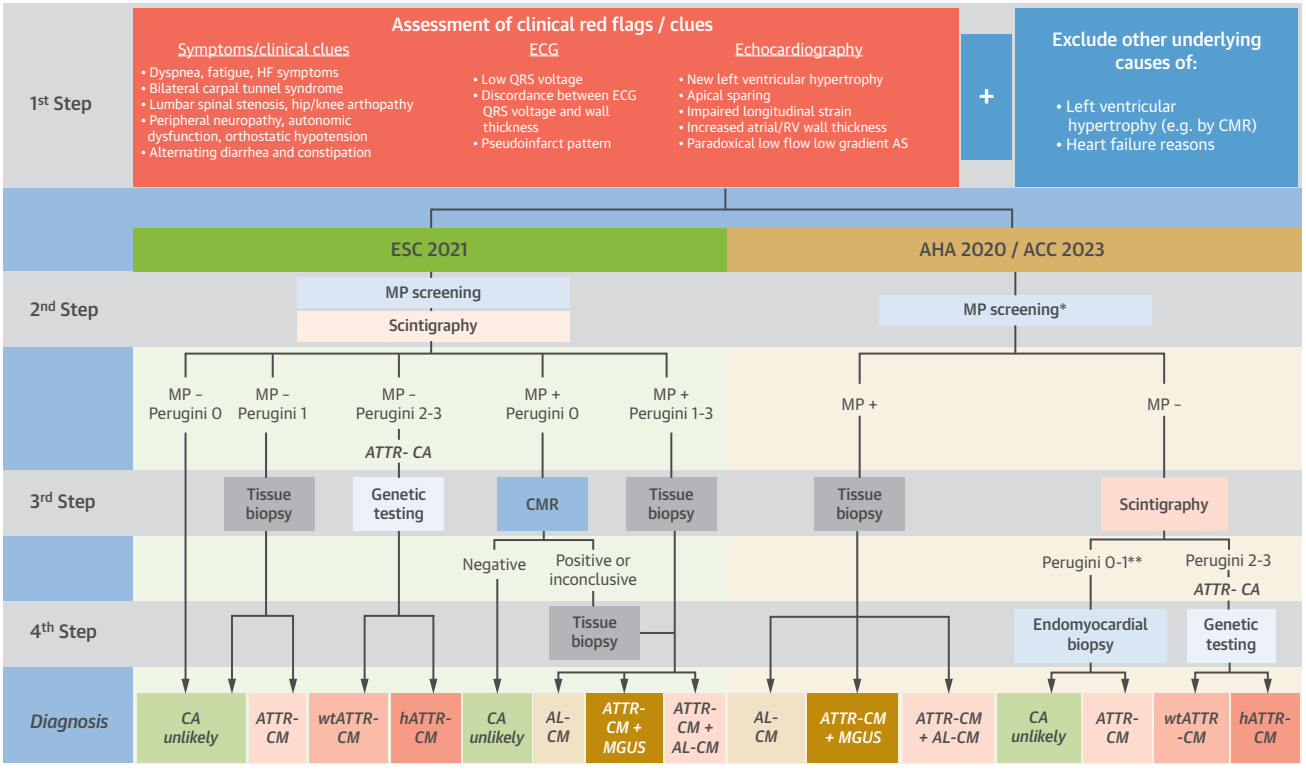

*ACC 2023 consensus recommended that cardiac scintigraphy could be ordered simultaneously for efficiency but must be interpreted in the context of the negative monoclonal protein screen. **ACC 2023 consensus recommended "considering" biopsy if scan result is negative or equivocal but clinical suspicion is high, to avoid false negative results. ACC = American College of Cardiology; AHA = American Heart Association; AL-CM = amyloid light-chain cardiomyopathy; AS = aortic stenosis; ATTR-CM = amyloid transthyretin cardiomyopathy; CA = cardiac amyloidosis; CMR = cardiac magnetic resonance; ECG = electrocardiography; ESC = European Society of Cardiology; hATTR-CM = hereditary amyloid transthyretin cardiomyopathy; HF = heart failure; MGUS = monoclonal gammopathy of undetermined significance; MP = monoclonal protein; RV = right ventricular; wtATTR-CM = wild-type amyloid transthyretin cardiomyopathy.

undetermined significance, which requires hematology assessment. If uncertainty of its possible causative role in amyloid CM still exists after such assessment, endomyocardial biopsy may still be required.[7-9] Although the present algorithms provide guidance on how to incorporate current imaging methods into the downstream testing process for accurately diagnosing ATTR-CM and its subtypes, it is important for the treating physician to understand the different aspects of each imaging modality.

COMPARISON OF MULTIMODALITY CARDIAC IMAGING METHODS IN ATTR-CM

ECHOCARDIOGRAPHY. Compared with other modalities, echocardiography is widely available and uniquely positioned to readily quantify LV wall thickness or mass and simultaneously assess cardiac dimensions and function, including diastolic filling patterns, all of which can be impaired in ATTR-CM.[13] Although a prevailing understanding of the pathophysiology of ATTR-CM suggests that amyloid fiber deposition occurs from basal to apical and from subendocardial to epicardial regions, affecting longitudinal biventricular function (influenced by subendocardial myocardial fibers), this concept has not yet been supported by evidence-based studies. Therefore, it remains ambiguous how longitudinal function is the initial impaired parameter and how the pattern commonly referred to as "apical sparing" or "cherry on top" in global longitudinal strain (GLS) imaging (ie, high ratio of apical longitudinal strain to the sum of base and mid longitudinal strain [RELAPS]) manifests in ATTR-CM (**Figure 2**).[14] It is important to note that apical sparing in echocardiography can be present in other LV hypertrophic

JACC: CARDIOVASCULAR IMAGING, VOL. 17, NO. 2, 2024
FEBRUARY 2024:195–211

FIGURE 2 Clinical Example of Multimodality Imaging in Amyloid Transthyretin Cardiomyopathy

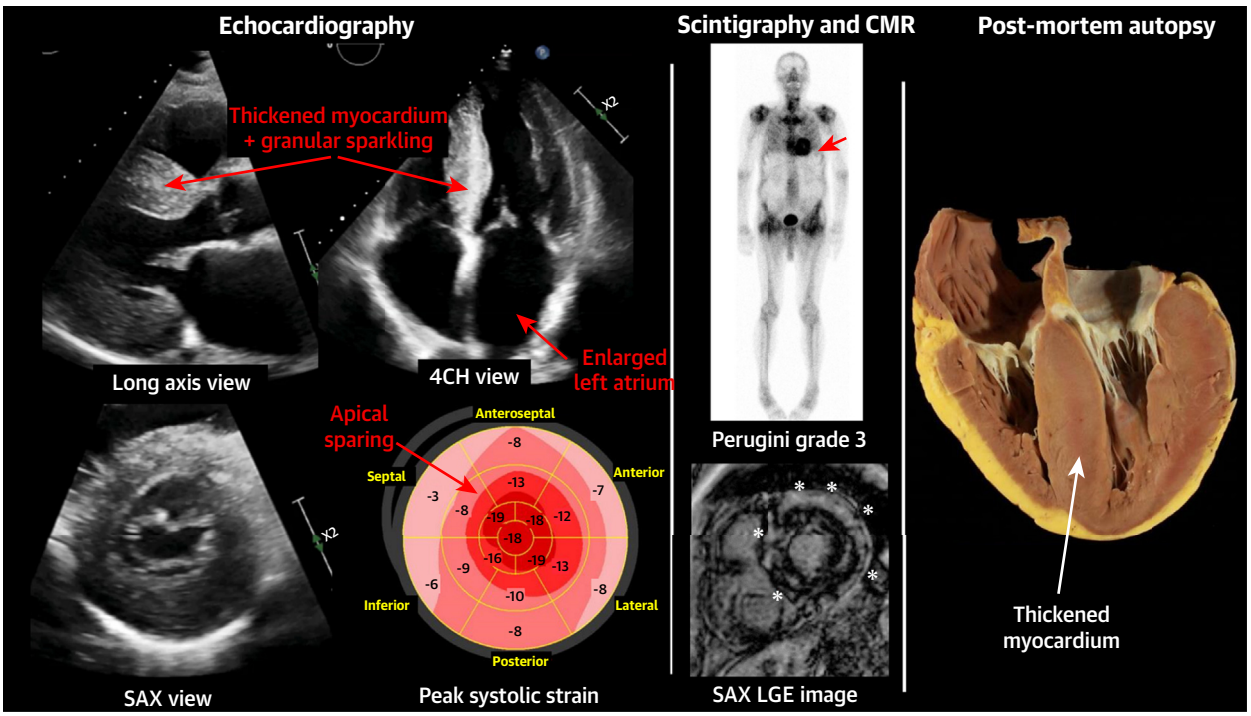

Clinical example of a 74-year-old man who presented with progressive dyspnea (ie, NYHA functional class III) and a markedly elevated N-terminal pro-B-type natriuretic peptide value of 2,805 pg/mL. Laboratory testing and immunofixation results were negative for light-chain amyloidosis. Transthoracic echocardiography revealed significant left ventricular hypertrophy, an enlarged left atrium, granular sparkling, apical sparing in peak longitudinal strain imaging (preserved strain in the apex, compared with marked impaired strain in the basal segments), a left ventricular ejection fraction of 45%, restrictive diastolic function, and no significant valve disease. Scintigraphy showed amyloid transthyretin cardiomyopathy with Perugini grade 3, and extensive late gadolinium enhancement (LGE) was present in CMR, with characteristic difficult nulling of the myocardium. The patient died of heart failure during follow-up, and in the postmortem autopsy hypertrophic heart, amyloid transthyretin cardiomyopathy could be confirmed. 4CH = 4-chamber; SAX = short-axis; other abbreviation as in Figure 1.

conditions and that the accuracy highly depends on the cohort examined; the sensitivity and specificity of apical sparing as a clinical sign of suspected amyloidosis can therefore vary (Table 1).[7,15-30] Alternative measures have been suggested, including septal apical-to-base longitudinal strain (SAB), where a threshold greater >2.1 demonstrated moderate accuracy,[11] as well as the ratio of ejection fraction (EF) to GLS (EFSR).[31] This ratio can help to distinguish between ATTR-CM and non-ATTR CM (ie, HCM and hypertensive cases), thus indicating that a notably more maintained global function relative to a more compromised longitudinal myocardial deformation suggests the presence of ATTR-CM.[19] This is underlined by the finding that, in the critical subgroup of patients with an LV ejection fraction (LVEF) >55% and mild hypertrophy (ie, wall thickness of 12-16 mm), where disease overlap is common, EFSR outperformed other markers such as GLS, RELAPS, and SAB.[19] In fact, an EFSR >4.1 cutoff was found to have the highest diagnostic accuracy for ATTR-CM.[19] A recent study revealed that novel analysis of left ventricular mechanical deformation, focusing on alterations in twist and untwist rates, can detect these changes even before an increase in LV thickness becomes apparent. The findings highlight that rotational mechanics could serve as an early myocardial deformation marker for ATTR-CM.[32] Although echocardiography provides a valuable tool for assessment of LV function and structure (which can be altered in ATTR-CM), it cannot enable direct assessment of myocardial tissue characteristics as can be directly altered by amyloid deposition.

NUCLEAR IMAGING. Semiquantitative methods. Bone scintigraphy can image amyloid deposits and has emerged as a critically valuable imaging technique in the diagnosis of ATTR-CM, as highlighted in the recent recommendations.[3-5,7-9] Different tracers are available and commonly include technetium-99m (^{99m}Tc)-3,3-diphosphono-1,2-propanodicarboxylic acid

TABLE 1 Selected Studies Assessing Diagnostic Accuracies of Multimodality Imaging Parameters to Diagnose ATTR

First Author, Year	N	Study Group	ATTR, %	Reference Test	Parameter Assessed	Sensitivity, %	Specificity, %
Echocardiography							
Di Bella et al,[16] 2011	33	ATTR vs HCM, normal	33	Echocardiographic parameters and genetic test, scintigraphy ^{99m}TC-DPD	Epicardial circumferential strain ≤−8.1%	46	81
					Mean epicardial circumferential strain ≤−8.1% in >20% of LV segments	64	82
Phelan et al,[12] 2012	85	CA (ATTR, AL) vs AS, HCM, LVH	65	EMB, extracardiac biopsy, imaging, clinical data	RELAPS >1.0	93	82
Pagourelias et al,[19] 2017	100	CA (ATTR, AL) vs HCM, hypertensive cardiomyopathy	35% of CA patients, 15% of total group	EMB	GLS >−15.1	88	72
					GCS >−18.3	86	57
					GRS ≤9.01	66	89
					EFSR >4.1	90	92
					RELAPS >0.87	63	85
					RELAPS >1.0	38	93
					SAB >3.1	48	87
					SAB >2.1	65	53
Cuddy et al,[11] 2022	598	ATTR vs non-ATTR	47	EMB or bone scintigraphy, laboratory test	SAB >2.1	74	64
					RELAPS >1	7	99
					EFSR >4.1	83	43
Nuclear scintigraphy							
Haro-del Morral et al,[20] 2012	19	ATTR vs AL	42	EMB, genetic	^{99m}Tc-DPD Perugini score ≥2	100	100
Gillmore et al,[5] 2016	1,217	ATTR vs AL, other amyloidosis, suspected amyloidosis	70	EMB	^{99m}Tc-DPD, ^{99m}Tc-PYP, or ^{99m}Tc-HMDP Perugini score ≥1	99	68
					^{99m}Tc-DPD, ^{99m}Tc-PYP, or ^{99m}Tc-HMDP Perugini score ≥2	91	87
Moore et al,[21] 2017	21	ATTR vs AL	62	EMB, genetic	^{99m}Tc-DPD Perugini score ≥2	100	88
Capelli et al,[22] 2017	65	ATTR vs AL	60	EMB, extracardiac biopsy, genetic, imaging	^{99m}Tc-HMDP Perugini score ≥1	100	96
Treglia et al,[23] 2018	Meta-analysis (529 patients)	ATTR vs AL, other amyloidosis	Various	Biopsy, genetic, immunohistochemistry	Bone scintigraphy Perugini score ≥2	92	95
					^{99m}Tc-DPD Perugini score ≥2	95	88
					^{99m}Tc-PYP Perugini score ≥2	87	75
					^{99m}Tc-HMDP Perugini score ≥2	86	98
Brownrigg et al,[24] 2019	Meta-analysis (27 studies)	ATTR vs AL, hypertensive heart disease, HCM, lysosomal storage disease, nonischemic dilated cardiomyopathy	Various	ATTR vs non-ATTR	^{99m}Tc-DPD, ^{99m}Tc-PYP, or ^{99m}Tc-HMDP Perugini score ≥1	88	87
				EMB		82	99
				Extracardiac biopsy			
				ATTR vs AL	^{99m}Tc-DPD, ^{99m}Tc-PYP, or ^{99m}Tc-HMDP Perugini score ≥2	92	89
				EMB		91	97
				Extracardiac biopsy			

Continued on the next page

(DPD), ^{99m}Tc-pyrophosphate (PYP), or ^{99m}Tc-hydroxymethylene-diphosphonate (HMD), all offering high sensitivity for ATTR-CM diagnosis. In fact, in a pooled analysis including 6 studies, using biopsy and genotyping/immunohistochemistry as the reference standard, bone scintigraphy yielded a sensitivity of 92% and a specificity of 95% (ie, when using a visual Perugini score of ≥2) for ATTR-CM.[23] Further, the negative likelihood ratio of a normal bone scintigraphy scan is very low, thereby indicating that the test highly accurately can rule out ATTR-CM.[23] False negative scans are very rare and may occur in early-stage ATTR-CM disease, where amyloid infiltration is minimal (and perhaps not even clinically significant) or in patients with hereditary ATTR with certain pathogenic ATTR variants such as p.(Y134C).[23,24,33,34] The Perugini grading system, a visual score, graded from 0 (no cardiac uptake, negative scan) to grade 2 to 3, is used to visually report the degree of bone tracer uptake in the heart.[5] Although a positive scan result is predictive of adverse outcomes compared with a negative scan result, the prognostic significance of a grade 1 or 2 vs grade 3 is still debatable.[35] Expert guidelines for ^{99m}Tc-PYP/DPD/HMDP image acquisition recommend imaging 2 to 3 hours postinjection, with optional 1-hour imaging for experienced laboratories for ^{99m}Tc-PYP imaging.[33,35]

To prevent misinterpretation resulting from blood pool activity or uptake within the stomach, which is more likely in planar views, multiplanar imaging (eg, single-photon emission computed tomography [SPECT] or, ideally, fused with computed tomography [CT; SPECT/CT]) is crucial for distinguishing myocardial uptake from blood pool activity. Further misinterpreting tracer activity in the blood pool for myocardial uptake on planar images can occur if the

TABLE 1 Continued

First Author, Year	N	Study Group	ATTR, %	Reference Test	Parameter Assessed	Sensitivity, %	Specificity, %
CMR							
Dungu et al,[25] 2014	97	ATTR vs AL	53	Positive histology from any organ, EMB, imaging, genetic	QALE	82	76
					LR model (age and interventricular septum thickness) without QALE	85	88
					LR model with QALE	87	96
de Gregorio et al,[26] 2016	47	ATTR vs HCM, normal	34	Positive histology from any organ or bone scintigraphy, imaging, laboratory	TTR-CA and HCM:		
					LA reservoir 19%	0.69	0.94
					Contractile (pump) −1.1%	0.69	0.75
					Both groups and controls:		
					LA reservoir 20.05%	0.93	0.72
					Contractile (pump) −1.4%	0.93	0.59
Oda et al,[27] 2017	61	ATTR vs AL	84	Positive histology from any organ, genetic, clinical data	LV circumferential strain to detect CA	94	77
Martinez-Naharro et al,[28] 2019	271	ATTR vs HCM, asymptomatic mutation	80	EMB or combination with symptoms, echocardiography and bone scintigraphy, genetic	All patients T1 >1,048 ms	87	80
					All patients ECV >0.47	92	82
					ATTRm T1 >1,051 ms	87	82
					ATTRm ECV >0.47	92	82
					ATTRwt T1 >1,048 ms	86	80
					ATTRwt ECV >0.47	93	82
Brownrigg et al,[24] 2019	Meta-analysis (27 studies)	ATTR vs AL, hypertensive heart disease, HCM, lysosomal storage disease, nonischemic dilated cardiomyopathy	Various	Detection ATTR MRI vs EMB	LGE subendocardium	86	92
					LGE atria	74	91
				MRI vs organ histology	LGE subendocardium	80	94
					LGE LA	78	60
				ATTR-CM from AL MRI vs any organ histology	LGE RV	94	34
					LGE LV	99	11
					LGE subendocardium	28	48
					LGE transmural	74	56
Slivnick et al,[29] 2023	147	ATTR vs AL	61	EMB, positive histology from any organ or bone scintigraphy or presence of AL fibrils	LGE and Look-Locker CMR pattern with negative light chains entire cohort	73	98
					Biopsy	69	98
Ioannou et al,[30] 2023	296	ATTR vs AL	56	Subanalysis of Perugini grade = 1 vs positive histology from any organ, presence of AL fibrils	ECV <0.40 after exclusion of Ser77Tyr and AApoAI	100	100

^{99m}Tc = technetium-99m; AL = amyloid light-chain amyloidosis; AS = aortic stenosis; ATTR = cardiac transthyretin-related amyloidosis; CA = cardiac amyloidosis; CMR = cardiac magnetic resonance; DPD = 3,3-diphosphono-1,2 propanodicarboxylic acid; ECV = extracellular volume; EFSR = ejection fraction to global longitudinal strain ratio; EMB = endomyocardial biopsy; GCS = global circumferential strain; GLS = global longitudinal strain; GRS = global radial strain; HCM = hypertrophic cardiomyopathy; HMDP = hydroxymethylene-diphosphonate; LA = left atrial; LGE = late gadolinium enhancement; LR = linear regression; LV = left ventricular; LVH = left ventricular hypertrophy; MRI = magnetic resonance imaging; PYP = pyrophosphate; QALE = query amyloid late enhancement (sum of score of LV and RV LGE: LGE of LV base, mid-apex, according to extent in each slice, ie, no LGE = 0, patchy = 1, circumferential = 2, transmural = 3, and circumferential/transmural = 4, and if LGE in right ventricle is present = +6); RA = right atrial; RELAPS = relative apical sparing (ratio of apical longitudinal strain to the sum of base and midlongitudinal strain); RV = right ventricular; SAB = septal apical to base longitudinal strain; TTR-CA = transthyretin cardiac amyloidosis.

scan is done too early after radiotracer injection. Notably, the lack of tracer uptake in the ribs, particularly when using ^{99m}Tc-PYP, signals that the images were captured too soon to provide an interpretable scan.[33] For optimal review, ^{99m}Tc-PYP/DPD/HMDP chest images are viewed in transaxial, sagittal, and coronal projections. Be aware that reorienting to cardiac projections can be challenging in negative scans. With ^{99m}Tc-PYP in the myocardium, the scan should resemble a normal perfusion scan with minimal blood pool activity. For SPECT interpretation, it is recommended to use inverse gray or linear color scales, and SPECT/CT fusion shows CT in gray and SPECT in color.[33] The heart-to-contralateral lung (H/CL) ratio is calculated by comparing the average counts from the region of interest covering the whole cardiac silhouette with counts from a similarly sized region of interest placed over the opposite lung in planar images. This ratio typically aligns with the visual evaluation on SPECT and can be used as an additional tool to aid decision making.[33]

Quantitative methods. Although in ESC, AHA, and ACC guidelines, quantitative scintigraphy is currently not (yet) a criterion, it could potentially offer prognostic insights, similar to the extracellular volume (ECV) fraction used in CMR.[14] SPECT quantitative values can be calculated as standardized uptake values (SUVs) after the estimation of the specific activity in the detectable lesions (in Bq/mL), normalized to both injection time and volume of distribution. First

studies reported a strong correlation between SUV and visual Perugini scores that enabled the delineation of patients with and without ATTR-CM.[36,37] It seems, according to a recent meta-analysis, that quantitative SPECT has the highest specificity (97%) and may provide more accurate information on amyloid burden more than the planar visual grade (specificity: 96%) and the H/CL ratio (specificity: 93%).[38] However, there is currently no agreement-on a definitive SUV threshold that can effectively differentiate between patients with and without ATTR-CM.

CARDIAC MAGNETIC RESONANCE. Function and tissue characterization. CMR provides unique information that integrates function and tissue properties and is thus well suited to identify mechanisms of heart failure such as can occur in patients with ATTR-CM.[14,39] CMR assessment of LV dimension or function and LV mass is superior to echocardiography and is depicted from a short-axis LV stack (compared with extrapolated calculations from echocardiography).[14,39]

Strengths of CMR include insights derived from tissue features such as late gadolinium enhancement (LGE) and mapping, especially relevant for ATTR-CM cases.[40] This holds true even in cases of clinically suspected ATTR-CM without LV hypertrophy. In advanced ATTR-CM, the presence of extensive LGE with a subendocardial or transmural distribution serves as an indicator of diffuse involvement, whereas difficulty to "null" the myocardium is a pathognomonic sign of amyloidosis. LGE is present in a high percentage of patients with ATTR-CM and often involves not on the left ventricle but also the atria and the right ventricle. The presence of diffuse LGE on CMR in a noncoronary distribution, particularly in the presence of abnormal nulling, provides a high diagnostic yield for cardiac amyloidosis, with a sensitivity more than 85% in a pooled analysis,[24] and it may further provide prognostic information.[41]

Myocardial T1 relaxation time can be quantified by T1 mapping as either a precontrast (native) value or by using an additional postcontrast image to calculate ECV, which is a surrogate for the expansion of the extracellular space resulting from amyloid deposition.[42] According to the consensus statement by the Society for Cardiovascular Magnetic Resonance, it is important to note that T1 mapping and ECV must be interpreted relative to institutional normative ranges because of differences across CMR scanning systems.[40] Native T1 values are increased in areas of amyloid deposition and correlate well with markers of systolic and diastolic dysfunction in ATTR-CM.[43] The normal ECV usually ranges between 22% and 32%, and ECV is elevated more than 40% in most patients with ATTR-CM, thus closely correlating with disease stages.[43-45] In fact, T1 mapping and ECV showed both, with an AUC of 0.87 and 0.91, high diagnostic accuracy for ATTR-CM against HCM subjects when using bone scintigraphy as the reference standard.[28] The T1 cutoff value to diagnose definitive or possible cardiac ATTR was 1,048 ms, with a specificity of 80% and a sensitivity of 87%; for ECV, the cutoff value was 0.47, with a specificity of 82% and a sensitivity of 92%.[28] After adjusting for established predictors such as Perugini grade and LGE, ECV inherits independent predictive information in ATTR-CM (**Central Illustration**)[28,43,45,46] and might be the earliest disease marker to track amyloid deposition.

Of note, there are ATTR-CM cases with normal T1 mapping values, elevated ECV and elevated LV mass (ie, T1 vs ECV paradox). The ongoing conversation is centered on whether this paradox can be explained by considering the ratio of total intracellular mass to total extracellular mass. Specifically, it is hypothesized that the extracellular density of the myocardium may be much higher if there is an accumulation of extracellular "protein" compared with the traditional density values used in volume-based calculations for the left ventricle.[28,47] Further, T2 mapping does not provide specific findings in ATTR-CM but can be generally helpful to differentiate edema from fibrosis in cases of elevated T1.[48]

In summary, ECV should be used as the primary imaging marker in ATTR-CM for diffuse fibrosis assessment because it demonstrates better diagnostic accuracy compared with LGE, and it seems to be the superior prognostic marker for adverse events compared with both LGE and native T1. Although native T1 mapping may provide some additional information, it has to be used with caution when it is a single parameter because there are ATTR-CM cases reported with normal T1 mapping but elevated ECV.[28]

Strain CMR. Similar to echocardiography, decreased LV GLS in ATTR-CM can be assessed using CMR-based strain analysis.[49] In various orientations (ie, radial, circumferential, longitudinal), myocardial strain can be depicted from routinely acquired CMR cine images by using a postprocessing feature-tracking technique or CMR tagging with high reproducibility.[50] In a study by Oda et al,[27] an LV global circumferential strain comparison between patients with LGE-positive and LGE-negative systemic amyloidosis revealed 94% sensitivity, 77% specificity, and 90.2% accuracy in identifying LGE-positive amyloidosis by using CMR strain.[27] Furthermore, LV circumferential strain

JACC: CARDIOVASCULAR IMAGING, VOL. 17, NO. 2, 2024
FEBRUARY 2024:195–211

CENTRAL ILLUSTRATION **Contemporary and Future Role of Multimodality Cardiac Imaging in Cardiac Transthyretin-Related Amyloidosis**

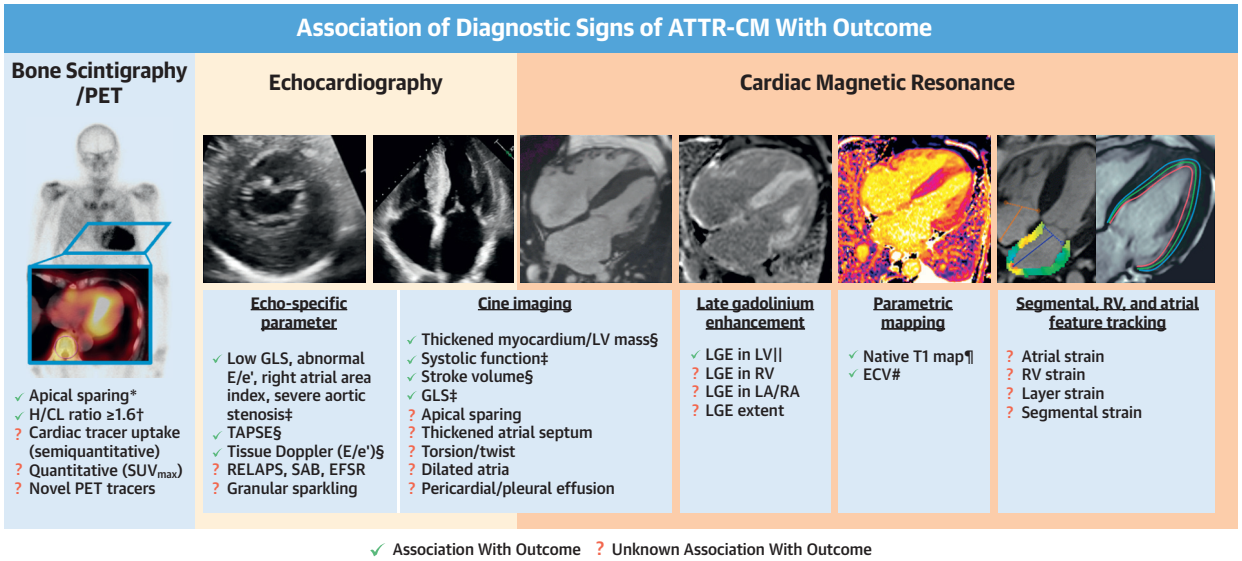

Alwan L, et al. J Am Coll Cardiol Img. 2024;17(2):195–211.

The different diagnostic modalities (ie, echocardiography, scintigraphy, positron emission tomography (PET), and cardiac magnetic resonance) for amyloid transthyretin cardiomyopathy (ATTR-CM) and their parameters are depicted. Some of the features have been studied and correlate with outcome, whereas the associations of other and novel parameters with outcome are unknown. *Sperry BW, Vranian MN, Tower-Rader A, et al. Regional variation in technetium pyrophosphate uptake in transthyretin cardiac amyloidosis and impact on mortality. *J Am Coll Cardiol Img.* 2018;11:234-242.†Castano A, Haq M, Narotsky DL, et al. Multicenter study of planar technetium 99m pyrophosphate cardiac imaging: predicting survival for patients with ATTR cardiac amyloidosis. *JAMA Cardiol.* 2016;1:880-889. ‡Chacko L, Martone R, Bandera F, et al. Echocardiographic phenotype and prognosis in transthyretin cardiac amyloidosis. *Eur Heart J.* 2020;41:1439-1447. §Knight DS, Zumbo G, Barcella W, et al. Cardiac structural and functional consequences of amyloid deposition by cardiac magnetic resonance and echocardiography and their prognostic roles. *J Am Coll Cardiol Img.* 2019;12:823-833. ||Fontana M, Pica S, Reant P, et al. Prognostic value of late gadolinium enhancement cardiovascular magnetic resonance in cardiac amyloidosis. *Circulation.* 2015;132:1570-1579. ¶Pan JA, Kerwin MJ, Salerno M. Native T1 mapping, extracellular volume mapping, and late gadolinium enhancement in cardiac amyloidosis: a meta-analysis. *J Am Coll Cardiol Img.* 2020;13:1299-1310. #Martinez-Naharro A, Treibel TA, Abdel-Gadir A, et al. Magnetic resonance in transthyretin cardiac amyloidosis. *J Am Coll Cardiol.* 2017;70:466-477. ECV = extracellular volume fraction; E/e′ = ratio of early diastolic transmitral flow velocity to early diastolic mitral annular velocity; EFSR = ratio of ejection fraction to global longitudinal strain; GLS = global longitudinal strain; H/CL = heart-to-contralateral lung ratio; LA = left atrium; LGE = late gadolinium enhancement; LV = left ventricle; RA = right atrium; RELAPS = ratio of apical longitudinal strain to the sum of base and midlongitudinal strain; RV = right ventricle; SAB = septal apical-to-base longitudinal strain; SUV_{max} = maximum standardized uptake value; TAPSE = tricuspid annular plane systolic excursion.

correlated with the severity of cardiac amyloid infiltration and may be more sensitive than LGE for the identification of early cardiac involvement in patients with ATTR-CM.[27] The utility of a novel strain parameter such as segmental, regional, layer strain or right atrial, left atrial, and right ventricular strain in improving the diagnosis and prognosis of patients with ATTR-CM is an avenue of future research.

Novel CMR markers. Myocardial stiffness in patients with ATTR-CM has a significant impact on cardiac function and limits diastolic filling, thus resulting in heart failure symptoms. CMR elastography is a noninvasive imaging technology that uses shear wave propagation to image and evaluate the stiffness of soft tissue. Recent studies using magnetic resonance elastography to quantify LV stiffness demonstrated that myocardial stiffness in patients with ATTR-CM was considerably higher than in healthy control subjects.[51,52]

Magnetic resonance spectroscopy is another novel technique, and it enables the assessment of metabolites, including triglycerides and creatine. In the healthy human heart, fatty acid β-oxidation produces energy that requires triglyceride storage. Reduced triglyceride use is associated with advanced-stage heart failure.[53] Gastl et al[54] reported the detection of decreased myocardial triglyceride levels in patients with ATTR-CM and functional cardiac impairment. This phenomenon appeared to correlate with the degree of myocardial thickening and LV strain, but

TABLE 2 Multimodality Imaging in Prognostication and Guiding/Monitoring ATTR-CM Therapy

Imaging Modality	Prognosis	Utility for Treatment Monitoring	Limitations
Echocardiography	• Parameters associated with worse prognosis include low GLS, abnormal E/e′, right atrial area index, severe aortic stenosis[13] • Strain from 4 chambers (ie, LV GLS, LA/RV strain, RV strain) are associated with outcome[62] • LV myocardial work indices are more impaired in CA compared with healthy subjects with prevalent basal and medium segment impairment compared with relatively spared apical ones[63]	• Appropriate to repeat echocardiography in ATTR-CM with worsening cardiac symptoms[8] • Indicative of disease progression: ≥5% decrease in LVEF, ≥5 mL decrease in SV or ≥1% increase in GLS[64]	• Data suggest that SV index is prognostic and similar to left LV strain in AL amyloidosis, independent of biomarker staging in AL amyloidosis patients,[65] and may therefore hold true for ATTR-CM. Because SV index is routinely calculated and widely available, it could serve as the preferred echocardiographic measure to predict outcomes
Myocardial scintigraphy	• Apical sparing and increased mortality in ATTR-CM dependent on the regional distribution of tracer uptake[66] • H/CL ratio of >1.5 is associated with higher mortality[67]	• Under discussion, whether ^{99}mTc-PYP/DPD can be used for monitoring response to therapy[68]	• Serial ^{99m}Tc-PYP scanning may not correlate with clinical progression[69] • Expertise needed: ^{99m}Tc-PYP: false positives or false negatives if performed incorrectly[70]
Positron emission imaging		• ^{11}C-PIB,^{18}F-florbetapir, and ^{18}F-florbetaben use may be a potential method to monitor CA patients and measure and response to treatment[71-74]	• Only limited data available
CMR	• LGE proved to be independently associated with outcome[41] • Transmural LGE predicted death and remained independent after adjustment for N-terminal pro-B-type, ejection fraction, SV index, E/e′, and LV mass index[41] • ECV showed stronger correlations with systolic and diastolic function and ECV ≥0.59 was associated with poor prognosis[46] • ECV is a better predictor for outcome than T1 mapping and LGE in ATTR-CM[4,45] • ECV elevations precede the development of LGE in cardiac amyloidosis and may allow diagnosis at earlier disease stages[75]	• Because ECV is able to quantify the degree of expansion of the interstitium, its role as a useful marker for monitoring treatment response in ATTR-CM is under discussion • In patients with ATTR-CM, ECV has been shown to increase less in the response to patisiran treatment group compared with the placebo group[68]	• It is unclear how T1 mapping and ECV can be used for documenting treatment response at various stages or different time points because ATTR-CM shows a nonlinear course • Timing of repeat CMR for monitoring is unclear because structural changes in response may be nonlinear

ATTR-CM = transthyretin amyloid cardiomyopathy; AI = artificial intelligence; E/e′ = ratio of early diastolic transmitral flow velocity to early diastolic mitral annular velocity; MDP = methylenediphosphonic acid; SV = stroke volume; T1 = longitudinal relaxation time; 11C-PiB = 11C-Pittsburgh B; other abbreviations as in Table 1.

not with LVEF. The ratio of triglyceride to water (TG/W ratio) did not correlate with body mass index, blood lipid levels, or age, findings suggesting that the TG/W ratio may be associated the accumulation of amyloid proteins. This suggestion is supported by a known histologic association between amyloid and the degree of fibrosis.[55]

CMR diffusion tensor imaging (DTI) has become a novel technique for determining the orientation of cardiac fibers.[56,57] It enables the investigation of water diffusion inside the tissue and the generation of additional scalar metrics for measuring structural integrity with regards to its orientation and angles, such as mean diffusivity (ie, freedom of water diffusion within the myocardium) and fractional anisotropy (ie, isotropic—unrestricted or equally restricted in all directions).[58] Another study applied CMR DTI in ATTR-CM to assess microstructural alterations and their consequences for myocardial function compared with healthy control subjects and found that the scalar DTI metrics of mean diffusivity and fractional anisotropy were significantly altered in ATTR-CM.[59] Mean diffusivity strongly correlated with native T1 mapping, whereas fractional anisotropy significantly correlated with ECV in the patients with ATTR-CM. Further, CMR DTI showed pronounced circumferential orientation of the myofibers in patients with ATTR-CM a feature that may provide the rationale for the reduction of certain strain values that occurs in such patients. Khalique et al[60] showed similar results and further evaluated sheetlet orientation (E2A, ie, the index of mean intravoxel sheetlet angle—the reorientation during LV thickening), which could distinguish patients with ATTR-CM from control subjects. Therefore, novel CMR markers such as magnetic resonance elastography, spectroscopy and DTI can capture specific features of amyloid infiltration and myocardial mechanics that may provide a deeper understanding of the microstructural consequences of ATTR-CM in the future.

THE ROLE OF MULTIMODALITY IMAGING TO GUIDE TREATMENT AND MONITOR ATTR-CM

Highly effective treatments for ATTR-CM come at a substantial cost, and even though tafamidis has been

TABLE 3 Evolving Application of AI in ATTR-CM Multimodality Imaging

First Author, Year	Modality and No. of Patients	Target	Task	References Standards
Echocardiography				
Zhang et al, 2018[84]	Echocardiography 14,035 studies	Fully automated echocardiogram interpretation	1) View identification (23 views) 2) Image segmentation (cardiac chamber) trained on 791 3) Quantification of structure and function 4) Disease detection (binary classification) (260 HCM, 81 CA, and 117 PAH)	Registry and guideline
Goto et al, 2021[89]	Echocardiography 5,843 studies (CA 1,863)	Automatic CA detection using electrocardiograms and echocardiograms	Classification (binary)	Imaging, laboratory, biopsy, genetic
Hudo et al, 2021[85]	Echocardiography 60,638 patients (10,744 ATTR-CM): Model development on 2,142 (1,071 ATTR-CM) External test: 58,478 (9,673 ATTR-CM)	Identifying patients at risk for wild-type ATTR-CM	Classification (binary)	Imaging, laboratory, biopsy, genetic and guidelines, and registry
Goto et al, 2022[90]	Echocardiography 8,392 patients	Improve hypertrophy detection performance in FL compared with single center	Classification (binary) HCM from AS, hypertension, and CA	Registry and guideline, biopsy, laboratory, genetic, imaging
Bonnefous et al, 2021[91]	Echocardiography 345 AL, 263 ATTRv, 402 ATTRwt, and 384 no amyloidosis	CA subtypes by unsupervised clustering	Unsupervised clustering	Imaging, scintigraphy,
Cotella et al, 2023[92]	Echocardiography 51 patients (36 ATTR-CM)	Automated assessment of LVEF and GLS	Segmentation and automated LVEF and GLS calculation from 2- and 4-chamber views	Registry and guideline
Nuclear medicine				
Santarelli et al, 2021[93]	PET ^{18}F-florbetaben 47 patients including: 13 ATTR (312 slices) 15 AL (375 slices) 19 control (420 slices)	CA classification from early acquired PET	Classification (multiclass)	Imaging, clinical, laboratory, bone scintigraphy and histologic, biopsy
Halme et al, 2022[88]	SPECT Scintigraphy ^{99m}Tc-HMDP 1,334 patients (47 ATTR-CM)	ATTR-CM Detection: grade <2 vs grade ≥2 grade <3 vs grade 3 Classification: Perugini grades	Detection (binary) Classification (multiclass)	Visually graded using Perugini scores (grades 0–3) Patients with grade ≥2 as ATTR-CM
Delbarre et al, 2023[87]	SPECT scintigraphy ^{99m}Tc-DPD/^{99m}Tc-HMDP 4,681 patients (383 ATTR-CM) Model development on 3,048 patients (281 ATTR-CM) External test 1,633 patients (102 ATTR-CM)	Detect ATTR-CM Perugini grade ≥2	Classification (binary)	Visual scoring of Perugini
Computed tomography				
Iacono et al, 2023[94]	Computed tomography (with contrast) 30 patients (15 CA)	Differentiation of CA from AS	Classification (binary)	Biopsy, bone scintigraphy, imaging
Cardiac magnetic resonance				
Satriano et al, 2020[95]	CMR (cine and LGE) 163 patients (85 HCM, 30 HTNcm, 30 AFD, and 18 CA)	Classify different HCM phenotype	Classification (binary)	Imaging, clinical, laboratory, bone scintigraphy
Martini et al, 2020[96]	CMR (LGE) 206 patients (107 CA, 57 ATTR-CM)	Diagnosis of CA	Classification (binary)	Imaging, clinical, laboratory, bone scintigraphy, histologic, biopsy
Agibetov et al, 2021[97]	CMR (LGE, MOLLI, cine) 502 patients (82 CA)	Automatically diagnose patients with CA	Classification (binary)	AL-CM, myocardial biopsy ATTR-CM, endomyocardial biopsy Laboratory tests
Germain et al, 2021[98]	CMR (cine) 241 patients (119 CA; 38 ATTR-CM)	Discriminate cardiac amyloidosis from LVH	Classification (binary)	Imaging, clinical, biologic, bone scintigraphy, and anatomical/histologic
Germain et al, 2023[86]	CMR (cine, LGE) 120 patients (50 ATTR-CM)	Classify AL vs ATTR-CM	Classification (binary)	Clinical, laboratory, imaging, biopsy

2D = 2-dimensional; 3D = 3-dimensional; AFD = Anderson-Fabry disease; ATTRv = hereditary variant transthyretin amyloidosis; ATTRwt = wild-type transthyretin amyloidosis; AUC = area under the curve; CNN = convolutional neural network; CV = cross validation; DL = deep learning; EHR = electronic health record; FL = federated learning; GBM = gradient boosting machine; Grad-CAM = gradient-weighted class activation mapping; HTNcm = hypertensive cardiomyopathy; IOU = intersection over union; MAD = median absolute deviation; MDA = myocardial deformation analysis; ML = machine learning; MLP = multilayer perceptron; MOLLI = modified Look-Locker inversion recovery; PAH = pulmonary arterial hypertension; PCA = principal component analysis; RF = random forest; SHAP = SHapley Additive exPlanations; VGG = Visual Geometry Group; WBS = whole body scan; other abbreviations as in Tables 1 and 2.

Continued on the next page

TABLE 3 Continued

Model Input Segmentation	Feature Type	AI Model	Scanner/Center Interpretability	Type of Evaluation	Best Performance
Echocardiography					
Multichannel image Manual segmenting	End-to-end training	DL-CNN	Multiscanner Multicenter None	1) 5-fold CV (277 patients) 2) External test (8,666 patients) 3) External test (8,666 patients) 4) 5-fold CV (458 patients)	1) Accuracy: 0.84 2) IOU: 0.64-0.89 3) MAD: 6-17% 4) CA AUC: 0.87
Video of echocardiogram as 3D input No segmentation	End-to-end training	DL-3D CNN	Multiscanner Multicenter None	30% internal test (1,422 patients) 4 external centers (441, 369, 229 and 239)	AUC internal test: 0.96 AUC of external test: 0.91, 0.89, 1.0, and 0.96
EHR Handcrafted conventional echocardiographic parameters No segmentation	Tabular data set from EHR	ML (LR, RF, and XGBoost)	Multiscanner Multicenter None	20% internal test External test : patients (ATTR) 34 6 (173), 14,596 (7,296), 3,886 (1,943), and 39,654 (261)	AUC internal test: 0.93 AUC eternal test: 0.95, 0.76, 0.78, and 0.80
30 frame videos as 3D images No segmentation	End-to-end training	DL-3D CNN	Multiscanner Multicenter Grad-CAM	Internal test from 3 centers (412, 243, and 421) External test: 3,040	AUC internal test FL: 0.91, 0.92 and 0.90 AUC external test: set 0.96
EHR and quantitative parameters of echocardiography No segmentation	Tabular data set	PCA and artificial neural network-based self-organizing maps	Single-scanner Single-center None	None	7 key clinical profiles identified associated by CA diagnosis and prognosis
Available trained network (ready-to-use DL model) Manual segmentation	Ready-to-use DL model	Ready-to-use DL model	Single-scanner Single-center None	Evaluation on whole data (51 as an external test)	No significant differences between manual and automated measurement
Nuclear medicine					
1,107 2D slices of PET No segmentation	End-to-end training	DL-CNN	Single-scanner single-center Activation map	Train and test split of 2D slices (110 2D test set) No external test	ATTR: Sensitivity: 0.935 Specificity: 0.897 Accuracy: 0.972
2D scintigraphy image No segmentation	End-to-end training	DL-CNN VGG16, ResNet50, InceptionV3, MobileNet, and 2 customized CNN	Multiscanner Multicenter Maximum activation maps	5-fold CV No external test	AUC: 0.87 for multiclass classification AUC: 0.94 for grade <2 vs grade ≥2 AUC 0.89 for grade <3 vs grade 3
2D WBS of scintigraphy No segmentation	End-to-end training	DL-CNN	Multiscanner Dual-center Activation map	5-fold CV on development data External test: 1,633 (102)	For both CV and external test set AUC: 0.99
Computed tomography					
Tabular radiomics feature set LV wall manual segmentation	Radiomics features (shape, intensity, and texture)	Different feature selection and classifier	Single-scanner Single-center SHAP	Leave 1 out CV No external test	Accuracy, sensitivity, and specificity of 0.93
Cardiac magnetic resonance					
3D-MDA Automated LV myocardium segmentation	Tabular 917 segmental architectural and deformation-based features	ML-MLP fully connected	Single-scanner Single-center None	5-fold CV No external test	AUC: 0.94
For ML in LV and RV volumes, mass and global function calculated and also visually assessed Automated 17-segment segmentation for tabular data.	Tabular conventional parameters for ML Short-axis 2,4 chamber images for DL	DL-CNN for image ML-based for tabular (GBM)	Multiscanner Single-center Grad-CAM	Splitting 20% test set No external test	AUC DL: 0.98 AUC ML: 0.95
Single 2D slice for image-based analysis Average voting across all 2D slices for patient-based analysis No segmentation	From scratch (end-to-end training) Fine-tuning (end-to-end training) Feature extraction (using VGG16)	DL- CNNs VGG16 ML-LR classifier for feature extraction scenario	Single-scanner Single-center None	10-fold CV No external test	LGE: patient-based AUC: 0.96 feature extraction MOLLI: patient-based AUC: 0.93 fine tune Cine: Patient-based AUC: 0.91 feature extraction
Different shape and regions (cropped) with and without segmentation Single 2D slice for image-based analysis Average voting across all 2D slices for patient-based analysis Epicardial and myocardial segmentation in diastole and systole frames	End-to-end training From diastole and systole frames	DL-CNN VGG16	Dual-scanner Single-center Grad-CAM	40% held-out test set No external test	Frame-based AUC: 0.82 Patient-based AUC: 0.93
Frame-based prediction and averaging for each patient 3 different views No segmentation	End-to-end training	DL-CNN VGG16	Multiscanner Single-center Saliency map	5-fold CV No external test.	AUC: Cine: 0.83 LGE: 0.67 Cine and LGE averaging: 0.82

JACC: CARDIOVASCULAR IMAGING, VOL. 17, NO. 2, 2024
FEBRUARY 2024:195–211

shown to be an effective therapy in a pivotal clinical trial, the presentation of the disease is changing with earlier diagnosis, and it is imperative to use cardiac imaging to document treatment success and for monitoring the course of the disease. Because ATTR-CM, if untreated, is associated with progressive amyloid deposition and worsening serum biomarkers, serial imaging showing stability in cardiac function and structure in a patient receiving disease-specific treatment should be a marker of treatment efficacy. Echocardiography is the simplest method for longitudinal follow-up of LV dimension and function,[61] whereas CMR may offer additional information about structural changes in the myocardium. Changes in LV mass, T1 mapping, and ECV values in CMR may be helpful to assess the progress of ATTR-CM and the response to therapy (**Table 2**).[3,4,8,13,39,41,45,46,62-75]

In the tafamidis trial, the primary outcome focused on a clinical endpoint. Although echocardiographic alterations at follow-up were presented as an exploratory endpoint, CMR was not incorporated in the protocol.[64] It is under discussion whether ECV could be used as an optimal modality to monitor treatment response with tafamidis, patisiran,[68,76] or novel NI006 antibody treatment in patients with ATTR-CM.[77] In fact, Rettl et al[76] demonstrated that treatment with tafamidis was associated with stability in ECV, LV mass, LV function, and serum N-terminal pro-B-type natriuretic peptide more than an 8- to 12-month period compared with worsening of these parameters in a historical control of treatment-naive patients with ATTR-CM. However, the duration of treatment was insufficient to evaluate the impact on long-term cardiac structure and function, as well as correlation with outcomes. These results support previous findings by Fontana et al[68] and suggest that serial CMR with ECV may be feasible to monitor patients with ATTR-CM.

Importantly, future studies need to evaluate the evolution of ATTR-CM by using different mapping techniques to provide a deeper understanding of the pathophysiological mechanism in treated and untreated ATTR-CM. Whether serial bone scintigraphy can be used for assessing treatment response is under discussion.[68,77,78] However, this is very unlikely, especially given that even if bone scintigraphy shows improvement after a year of TTR therapy, CMR indicators mostly remain stable. This discrepancy can probably be attributed to bone imaging uptake reflecting recent amyloid deposits rather than the overall amyloid quantity.[68,77,78] Newer positron emission tomography tracers, such as ^{11}C-Pittsburgh B (^{11}C-PiB), ^{18}F-florbetapir, and similar beta-amyloid-binding compounds have been proven to bind to amyloid deposits with high affinity, and they are quantifiable and correlated with amyloid burden.[79] As a result, they offer a greater potential to measure the response to treatment. However, despite their importance in identifying ATTR-CM, so far these methods have not been investigated for disease monitoring.[71-74]

FUTURE ROLE OF AI IN MULTIMODALITY IMAGING IN ATTR-CM

In the realm of cardiac diseases, AI has gained significant attention, and ATTR-CM is no exception to this trend. However, before delving deeper into the application of AI in ATTR-CM, it is essential to clarify the fundamental concepts. AI is an umbrella term referring to computational algorithms that attempt to imitate human behaviors to carry out tasks requiring human intelligence,[80] whereas machine learning (ML), a subfield of AI, involves computational, mathematical, and statistical algorithms that aim to learn directly from data without the necessity of explicit programming.[80,81] Separate algorithms (ie, feature extraction, selection, reduction) are needed to conduct ML tasks using the conventional ML framework.[82] However, deep learning (DL) is an ML algorithm that consolidates all these steps into a single package, even without the need for some steps.[82] DL algorithms, which are mainly based on neural networks, attempt to mimic the human visual system behavior, by presenting different data abstraction levels in their architecture.[82] Various tasks in ATTR-CM, especially in cardiac imaging, can potentially be performed by ML algorithms, including detection (eg, identifying the cardiac regions), classification (eg, distinguishing between ATTR and AL), clustering (eg, discovering new LGE T1 patterns), segmentation (eg, segmenting of myocardial dimension), regression (eg, directly estimating LVEF), time-to-event prediction (eg, predicting outcomes for ATTR patients), image-to-image translation (eg, generating contrast from non-contrast-enhanced images, such as T1 mapping and ECV), and image captioning (generating a report from direct CMR analysis).[83] In fact, Zhang et al[84] demonstrated that AI in echocardiography is capable of taking more than several tasks through a fully automated ML pipeline for echocardiogram interpretation that includes diverse view identification, precise cardiac chamber segmentation, automated quantification, and even classification of different diseases with high accuracy, whereas Huda et al[85] showed that the ML algorithm, using a large multi-institutional electronic health record data set, identifies patients with ATTR-CM with

FIGURE 3 **Future Role of Artificial Intelligence in Improving Diagnostics and Outcome Prediction in ATTR-CM**

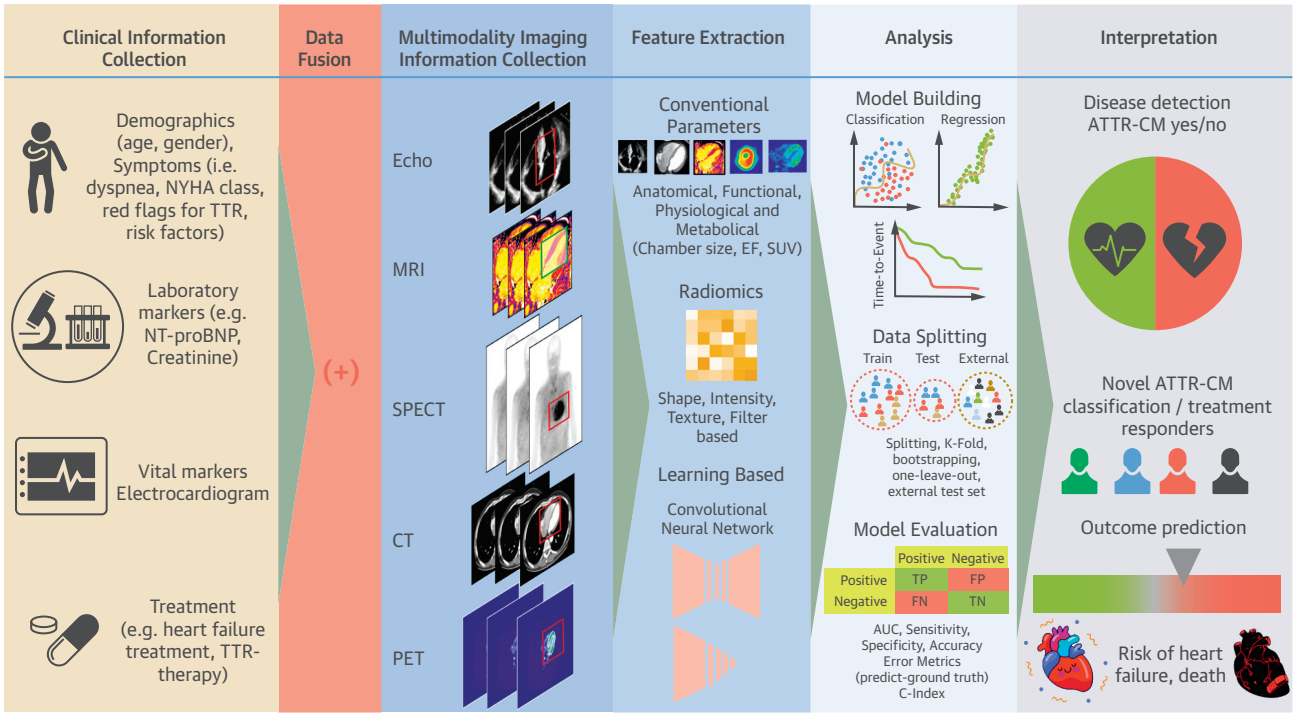

This figure summarizes the potential of AI in amyloid transthyretin cardiomyopathy (ATTR-CM) by combining clinical data with imaging data, novel classification, and improved prediction models for disease detection, treatment responder identification, and outcome prediction. AUC = area under the curve; CT = computed tomography; Echo = echocardiography; EF = ejection fraction; FN = false negative; FP = false positive; MRI = magnetic resonance imaging; PET = positron emission tomography; SPECT = single-photon emission computed tomography; SUV = standardized uptake value; TF = true negative; TP = true positive; TTR = transthyretin.

an AUC ranging from 0.76 to 0.95. Germain et al[86] reported an AUC of 0.83 and an AUC of 0.68 for the DL model by using cine and LGE sequences, respectively, for classifying AL vs ATTR-CM. Given the potential of AI to enhance accuracy and speed not just within echocardiography and CMR, Delbarre et al[87] and Halme et al[88] developed a DL-based classification model to identify Perugini grade from scintigraphy images, thus achieving an AUC of 0.87 to 0.99. Although some studies specifically focused on ATTR-CM imaging (**Table 3**),[84-98] another intriguing avenue involves the potential for AI to enhance the informational content of diagnostic images through advanced image analysis in combination with ECG, electronic health records, and clinical data sets for classification purposes. This could potentially streamline early detection of ATTR-CM and improve risk stratification and decision making, as depicted in **Figure 3**.

Notwithstanding the heightened expectations of AI, we must give careful consideration to the potential drawbacks and biases associated with AI, particularly when dealing with ATTR-CM. During ML algorithm development, various factors need to be considered to standardize the modeling process. Because the performance of ML algorithms depends on both the size and quality of the data,[99,100] collaborative endeavors should be undertaken to establish multicenter studies and registries, especially in a rare disease such as ATTR-CM. To develop a repeatable, fair, and generalizable model, not only are large, heterogeneous, and diverse data from multiple centers essential to avoid any potential bias,[101] but also external validation is needed to avoid data distribution shift issues. In 15 studies summarized in **Table 3**, only 5 studies used a multicenter data set[84,88-90] and/or an external validation set[84,85,87,89,90] for model development and evaluation (4 ultrasound and 1 nuclear medicine). Recently, federated learning (FL) algorithms have been proposed to address the obstacles in sharing data among different centers as a result of patient privacy ethical and legal issues by enabling ML model development across various centers without sharing the data set among different centers.[101] In ATTR-CM, Goto et al[90] highlighted the efficacy of FL in the ultrasound modality for the

JACC: CARDIOVASCULAR IMAGING, VOL. 17, NO. 2, 2024
FEBRUARY 2024:195–211

binary classification of HCM vs other diseases, including ATTR-CM. FL potentially could also benefit other imaging modalities and different tasks.

Another issue in ML model developments is the unbalanced nature of data in real clinical situations, most specifically in rare diseases such as ATTR-CM. Data augmentation techniques could partially address this issue; however, different evaluation metrics should be used to assess model performance.[99-101] One of the primary challenges of AI studies in ATTR-CM was the reporting of certain metrics that do not reflect the actual performance in such rare diseases. Another frontier to consider in ML model development is interpretability, given the black-box nature of ML.[100,101] Of 15 AI studies on ATTR-CM, 8 attempted to make the ML or DL models explainable by using various algorithms. AI models should be interpretable so we can understand the decision-making process (why and how), which could engender trust for further implementation in real clinical scenarios.[100,101]

To ensure the reproducibility of ML algorithms within the ATTR-CM imaging community, it is essential to document the model's parameters, hyperparameters, architecture, and sharing of code and data to improve model reproducibility.[100,101] Only 3 studies[84,85,89] (ultrasound modality) made their code or model publicly available. Moreover, data leakage during different steps of model development should be avoided, and the model should be evaluated in data sets rich in both size and diversity to ensure its statistical power.[100,101] Data splitting should be done on a per patient basis, not by slice or image, such as performed in the study by Santarelli et al,[93] to prevent potential data leakage into the test set. Most AI studies in ATTR-CM failed to detail the AI methodology steps, and none adhered to reporting the AI guidelines, such as the Proposed Requirements for Cardiovascular Imaging-Related Machine Learning Evaluation,[100] for medical image development. In addition, ML models should be compared with conventional algorithms to identify their added value because they need substantial resources, and reporting negative results and failures of standard ML models should be encouraged to provide a realistic representation and make physicians aware of potential biases.[99-101] Only 2 studies (CMR)[96,97] compared the performance of conventional ML and DL models in ATTR-CM.

AI could indeed play a significant role in future management of patients with ATTR-CM. However, considering the previously mentioned limitations and challenges, future research should concentrate on addressing these issues to maximize the full potential of AI application in ATTR-CM. Furthermore, although no studies have used AI for risk stratification so far, AI offers a potential avenue for future research in this domain. Finally, it is essential to evaluate AI models prospectively to enable their effective integration into actual clinical practice.

HIGHLIGHTS

- ATTR-CM is still an underrecognized entity, represented by accumulation of subtype-specific misfolded protein fibrils, which leads to progressive thickening of myocardial walls, impaired diastolic function, and restrictive CM, heart failure, and death.
- Recent European and American guidelines promote noninvasive imaging in combination with laboratory testing to establish the diagnosis of ATTR-CM.
- Future research in multimodality imaging holds the potential for deeper disease insight, treatment response monitoring, and improved outcome prediction. AI-based noninvasive image analysis and combining imaging and clinical data may provide more robust diagnostics, outcome prediction, and possible improvements of clinical decision making in the future.

CONCLUSIONS

At present, if clinical red flags or unexplained LV thickening are identified on echocardiography and/or CMR, in tandem with laboratory markers, bone scintigraphy serves as the noninvasive gold standard for diagnosing ATTR-CM. Future research in multimodality cardiac imaging is essential to better understand ATTR-CM progression and optimize patient selection for therapy in this clinical setting. As technology advances, the integration of AI-based imaging analysis and the application of AI to vast data sets encompassing clinical, laboratory, ECG, and multimodality cardiac imaging information present a promising avenue for potentially refining risk stratification in ATTR-CM.

FUNDING SUPPORT AND AUTHOR DISCLOSURES

This work was supported by the GAMBIT foundation. The Bern University Hospital (Inselspital Bern) has received grants from Pfizer for

the SWISS-CARE Amyloidosis registry. Dr Benz has received career development grants from the Swiss National Science Foundation; and has received reimbursement of travel expenses by Philips Healthcare and Amgen. Dr Cuddy has received research funding from Pfizer; has received honoraria for lectures from Ionis, BridgeBio, and Pfizer; and has received support for travel to meetings from Ionis. Dr Caobelli has received academic grant support from Mallinckrodt AG and Tillots AG; and has received speaker honoraria from Siemens Healthineers and Bracco. Dr Bernhard has received career development grants from the Swiss National Science Foundation. Dr Stämpfli has received consulting and speaker fees from Alnylam, Amgen, AstraZeneca, Bayer, Bristol-Myers Squibb, Pfizer, and Takeda. Dr Kwong has received research support from National Institutes of Health awards 1UH2 TR000901, 1RO1DK083424-01, and 1U01HL117006, Alnylam Pharmaceuticals, and the Society for Cardiovascular Magnetic Resonance. Dr Falk has received research funding from GlaxoSmithKline and Akcea; and has received consulting fees from Ionis, Alnylam Pharmaceuticals, and Caelum Biosciences. Dr Dorbala has received institutional grants from Pfizer, Attralus, GE Healthcare, Philips, the National Institutes of Health, and the American Heart Association; and has received payment for lectures from Janssen and Ionetix. Dr Gräni has received funding support from the Swiss National Science Foundation, InnoSuisse, the CAIM foundation, the GAMBIT foundation, and the Novartis Biomedical Research Foundation. All other authors have reported that they have no relationships relevant to the contents of this paper to disclose.

ADDRESS FOR CORRESPONDENCE: Dr Christoph Gräni, Department of Cardiology, Inselspital, Bern University Hospital, Freiburgstrasse 18, CH-3010 Bern, Switzerland. E-mail: christoph.graeni@insel.ch. @chrisgraeni.

REFERENCES

1. Tanskanen M, Peuralinna T, Polvikoski T, et al. Senile systemic amyloidosis affects 25% of the very aged and associates with genetic variation in alpha2-macroglobulin and tau: a population-based autopsy study. *Ann Med*. 2008;40:232–239.

2. Cornwell GG III, Murdoch WL, Kyle RA, Westermark P, Pitkänen P. Frequency and distribution of senile cardiovascular amyloid: a clinicopathologic correlation. *Am J Med*. 1983;75:618–623.

3. Ruberg FL, Grogan M, Hanna M, Kelly JW, Maurer MS. Transthyretin amyloid cardiomyopathy: JACC state-of-the-art review. *J Am Coll Cardiol*. 2019;73:2872–2891.

4. Dorbala S, Ando Y, Bokhari S, et al. ASNC/AHA/ASE/EANM/HFSA/ISA/SCMR/SNMMI expert consensus recommendations for multimodality imaging in cardiac amyloidosis: part 1 of 2—evidence base and standardized methods of imaging. *Circ Cardiovasc Imaging*. 2021;14:e000029.

5. Gillmore JD, Maurer MS, Falk RH, et al. Nonbiopsy diagnosis of cardiac transthyretin amyloidosis. *Circulation*. 2016;133:2404–2412.

6. Ioannou A, Patel RK, Razvi Y, et al. Impact of earlier diagnosis in cardiac ATTR amyloidosis over the course of 20 years. *Circulation*. 2022;146:1657–1670.

7. Kittleson MM, Maurer MS, Ambardekar AV, et al. Cardiac amyloidosis: evolving diagnosis and management: a scientific statement from the American Heart Association. *Circulation*. 2020;142:e7–e22.

8. Garcia-Pavia P, Rapezzi C, Adler Y, et al. Diagnosis and treatment of cardiac amyloidosis: a position statement of the ESC Working Group on Myocardial and Pericardial Diseases. *Eur Heart J*. 2021;42:1554–1568.

9. Kittleson MM, Ruberg FL, Ambardekar AV, et al. 2023 ACC expert consensus decision pathway on comprehensive multidisciplinary care for the patient with cardiac amyloidosis: a report of the American College of Cardiology Solution Set Oversight Committee. *J Am Coll Cardiol*. 2023;81:1076–1126.

10. Cipriani A, De Michieli L, Porcari A, et al. Low QRS voltages in cardiac amyloidosis: clinical correlates and prognostic value. *J Am Coll Cardiol CardioOnc*. 2022;4:458–470.

11. Cuddy SA, Datar Y, Ovsak G, et al. Optimal echocardiographic parameters to improve the diagnostic yield of Tc-99m-bone avid tracer cardiac scintigraphy for transthyretin cardiac amyloidosis. *Circ Cardiovasc Imaging*. 2022;15:e014645.

12. Phelan D, Collier P, Thavendiranathan P, et al. Relative apical sparing of longitudinal strain using two-dimensional speckle-tracking echocardiography is both sensitive and specific for the diagnosis of cardiac amyloidosis. *Heart*. 2012;98:1442–1448.

13. Chacko L, Martone R, Bandera F, et al. Echocardiographic phenotype and prognosis in transthyretin cardiac amyloidosis. *Eur Heart J*. 2020;41:1439–1447.

14. Knight DS, Zumbo G, Barcella W, et al. Cardiac structural and functional consequences of amyloid deposition by cardiac magnetic resonance and echocardiography and their prognostic roles. *J Am Coll Cardiol Img*. 2019;12:823–833.

15. Sun JP, Stewart WJ, Yang XS, et al. Differentiation of hypertrophic cardiomyopathy and cardiac amyloidosis from other causes of ventricular wall thickening by two-dimensional strain imaging echocardiography. *Am J Cardiol*. 2009;103:411–415.

16. Di Bella G, Minutoli F, Pingitore A, et al. Endocardial and epicardial deformations in cardiac amyloidosis and hypertrophic cardiomyopathy–2-d feature strain echocardiography. *Circ J*. 2011;75(5):1200–1208.

17. Liu D, Hu K, Niemann M, et al. Effect of combined systolic and diastolic functional parameter assessment for differentiation of cardiac amyloidosis from other causes of concentric left ventricular hypertrophy. *Circ Cardiovasc Imaging*. 2013;6:1066–1072.

18. Vergaro G, Aimo A, Barison A, et al. Keys to early diagnosis of cardiac amyloidosis: red flags from clinical, laboratory and imaging findings. *Eur J Prev Cardiol*. 2020;27:1806–1815.

19. Pagourelias ED, Mirea O, Duchenne J, et al. Echo parameters for differential diagnosis in cardiac amyloidosis: a head-to-head comparison of deformation and nondeformation parameters. *Circ Cardiovasc Imaging*. 2017;10:e005588.

20. De Haro-Del Moral FJ, Sánchez-Lajusticia A, Gómez-Bueno M, García-Pavía P, Salas-Antón C, Segovia-Cubero J. Role of cardiac scintigraphy with 99mTc-DPD in the differentiation of cardiac amyloidosis subtype. *Rev Esp Cardiol (Engl Ed)*. 2012;65:440–446.

21. Moore PT, Burrage MK, Mackenzie E, Law WP, Korczyk D, Mollee P. The utility of 99mTc-DPD scintigraphy in the diagnosis of cardiac amyloidosis: an Australian experience. *Heart Lung Circ*. 2017;26:1183–1190.

22. Cappelli F, Gallini C, Di Mario C, et al. Accuracy of 99mTc-hydroxymethylene diphosphonate scintigraphy for diagnosis of transthyretin cardiac amyloidosis. *J Nucl Cardiol*. 2019;26(2):497–504.

23. Treglia G, Glaudemans A, Bertagna F, et al. Diagnostic accuracy of bone scintigraphy in the assessment of cardiac transthyretin-related amyloidosis: a bivariate meta-analysis. *Eur J Nucl Med Mol Imaging*. 2018;45:1945–1955.

24. Brownrigg J, Lorenzini M, Lumley M, Elliott P. Diagnostic performance of imaging investigations in detecting and differentiating cardiac amyloidosis: a systematic review and meta-analysis. *ESC Heart Fail*. 2019;6:1041–1051.

25. Dungu JN, Valencia O, Pinney JH, et al. CMR-based differentiation of AL and ATTR cardiac amyloidosis. *J Am Coll Cardiol Img*. 2014;7:133–142.

26. de Gregorio C, Dattilo G, Casale M, Terrizzi A, Donato R, Di Bella G. Left atrial morphology, size and function in patients with transthyretin cardiac amyloidosis and primary hypertrophic cardiomyopathy-comparative strain imaging study. *Circ J*. 2016;80:1830–1837.

27. Oda S, Utsunomiya D, Nakaura T, et al. Identification and assessment of cardiac amyloidosis by myocardial strain analysis of cardiac magnetic resonance imaging. *Circ J*. 2017;81:1014–1021.

28. Martinez-Naharro A, Kotecha T, Norrington K, et al. Native T1 and Extracellular Volume in Transthyretin Amyloidosis. *J Am Coll Cardiol Img*. 2019;12:810–819.

29. Slivnick JA, Alvi N, Singulane CC, et al. Non-invasive diagnosis of transthyretin cardiac amyloidosis utilizing typical late gadolinium enhancement pattern on cardiac magnetic resonance and light chains. *Eur Heart J Cardiovasc Imaging*. 2023;24:829–837.

30. Ioannou A, Patel RK, Razvi Y, et al. Multi-imaging characterization of cardiac phenotype in different types of amyloidosis. *J Am Coll Cardiol Img*. 2023;16:464–477.

31. Pagourelias ED, Duchenne J, Mirea O, et al. The relation of ejection fraction and global longitudinal strain in amyloidosis: implications for differential diagnosis. *J Am Coll Cardiol Img*. 2016;9:1358–1359.

32. Cappelli F, Porciani MC, Bergesio F, et al. Characteristics of left ventricular rotational mechanics in patients with systemic amyloidosis, systemic hypertension and normal left ventricular mass. *Clin Physiol Funct Imaging*. 2011;31:159–165.

33. Khor YM, Cuddy SAM, Singh V, Falk RH, Di Carli MF, Dorbala S. (99m)Tc bone-avid tracer cardiac scintigraphy: role in noninvasive diagnosis of transthyretin cardiac amyloidosis. *Radiology*. 2023;306:e221082.

34. Rauf MU, Hawkins PN, Cappelli F, et al. Tc-99m labelled bone scintigraphy in suspected cardiac amyloidosis. *Eur Heart J*. 2023;44(24):2187–2198.

35. Hutt DF, Fontana M, Burniston M, et al. Prognostic utility of the Perugini grading of ^{99m}Tc-DPD scintigraphy in transthyretin (ATTR) amyloidosis and its relationship with skeletal muscle and soft tissue amyloid. *Eur Heart J Cardiovasc Imaging*. 2017;18:1344–1350.

36. Ross JC, Hutt DF, Burniston M, et al. Quantitation of ^{99m}Tc-DPD uptake in patients with transthyretin-related cardiac amyloidosis. *Amyloid*. 2018;25:203–210.

37. Caobelli F, Braun M, Haaf P, Wild D, Zellweger MJ. Quantitative ^{99m}Tc-DPD SPECT/CT in patients with suspected ATTR cardiac amyloidosis: feasibility and correlation with visual scores. *J Nucl Cardiol*. 2020;27:1456–1463.

38. Ahluwalia N, Roshankar G, Draycott L, et al. Diagnostic accuracy of bone scintigraphy imaging for transthyretin cardiac amyloidosis: systematic review and meta-analysis. *J Nucl Cardiol*. 2023;30:2464–2476. https://doi.org/10.1007/s12350-023-03297-1

39. Benz DC, Gräni C, Antiochos P, et al. Cardiac magnetic resonance biomarkers as surrogate endpoints in cardiovascular trials for myocardial diseases. *Eur Heart J*. 2023;44(45):4738–4747. https://doi.org/10.1093/eurheartj/ehad510

40. Messroghli DR, Moon JC, Ferreira VM, et al. Clinical recommendations for cardiovascular magnetic resonance mapping of T1, T2, T2* and extracellular volume: a consensus statement by the Society for Cardiovascular Magnetic Resonance (SCMR) endorsed by the European Association for Cardiovascular Imaging (EACVI). *J Cardiovasc Magn Reson*. 2017;19:75.

41. Fontana M, Pica S, Reant P, et al. Prognostic value of late gadolinium enhancement cardiovascular magnetic resonance in cardiac amyloidosis. *Circulation*. 2015;132:1570–1579.

42. Baggiano A, Boldrini M, Martinez-Naharro A, et al. Noncontrast magnetic resonance for the diagnosis of cardiac amyloidosis. *J Am Coll Cardiol Img*. 2020;13:69–80.

43. Fontana M, Banypersad SM, Treibel TA, et al. Native T1 mapping in transthyretin amyloidosis. *J Am Coll Cardiol Img*. 2014;7:157–165.

44. Mongeon FP, Jerosch-Herold M, Coelho-Filho OR, Blankstein R, Falk RH, Kwong RY. Quantification of extracellular matrix expansion by CMR in infiltrative heart disease. *J Am Coll Cardiol Img*. 2012;5:897–907.

45. Pan JA, Kerwin MJ, Salerno M. Native T1 mapping, extracellular volume mapping, and late gadolinium enhancement in cardiac amyloidosis: a meta-analysis. *J Am Coll Cardiol Img*. 2020;13:1299–1310.

46. Martinez-Naharro A, Treibel TA, Abdel-Gadir A, et al. Magnetic resonance in transthyretin cardiac amyloidosis. *J Am Coll Cardiol*. 2017;70:466–477.

47. Chamling B, Bietenbeck M, Drakos S, et al. A compartment-based myocardial density approach helps to solve the native T1 vs. ECV paradox in cardiac amyloidosis. *Sci Rep*. 2022;12:21755.

48. Bohnen S, Radunski UK, Lund GK, et al. Performance of t1 and t2 mapping cardiovascular magnetic resonance to detect active myocarditis in patients with recent-onset heart failure. *Circ Cardiovasc Imaging*. 2015;8(6):e003073.

49. Quarta CC, Solomon SD, Uraizee I, et al. Left ventricular structure and function in transthyretin-related versus light-chain cardiac amyloidosis. *Circulation*. 2014;129:1840–1849.

50. Fischer K, Linder OL, Erne SA, et al. Reproducibility and its confounders of CMR feature tracking myocardial strain analysis in patients with suspected myocarditis. *Eur Radiol*. 2022;32:3436–3446.

51. Arani A, Arunachalam SP, Chang IC, et al. Cardiac MR elastography for quantitative assessment of elevated myocardial stiffness in cardiac amyloidosis. *J Magn Reson Imaging*. 2017;46:1361–1367.

52. Chang IC, Arani A, Arunachalam SP, Grogan M, Dispenzieri A, Araoz PA. Feasibility study of cardiac magnetic resonance elastography in cardiac amyloidosis. *Amyloid*. 2017;24:161.

53. Neubauer S. The failing heart—an engine out of fuel. *N Engl J Med*. 2007;356:1140–1151.

54. Gastl M, Peereboom SM, Gotschy A, et al. Myocardial triglycerides in cardiac amyloidosis assessed by proton cardiovascular magnetic resonance spectroscopy. *J Cardiovasc Magn Reson*. 2019;21:1–10.

55. Mohammed SF, Mirzoyev SA, Edwards WD, et al. Left ventricular amyloid deposition in patients with heart failure and preserved ejection fraction. *J Am Coll Cardiol HF*. 2014;2:113–122.

56. Hales PW, Schneider JE, Burton RA, Wright BJ, Bollensdorff C, Kohl P. Histo-anatomical structure of the living isolated rat heart in two contraction states assessed by diffusion tensor MRI. *Prog Biophys Mol Biol*. 2012;110:319–330.

57. Nielles-Vallespin S, Mekkaoui C, Gatehouse P, et al. In vivo diffusion tensor MRI of the human heart: reproducibility of breath-hold and navigator-based approaches. *Magn Reson Med*. 2013;70:454–465.

58. McGill L-A, Scott AD, Ferreira PF, et al. Heterogeneity of fractional anisotropy and mean diffusivity measurements by in vivo diffusion tensor imaging in normal human hearts. *PLoS One*. 2015;10:e0132360.

59. Gotschy A, von Deuster C, van Gorkum RJ, et al. Characterizing cardiac involvement in amyloidosis using cardiovascular magnetic resonance diffusion tensor imaging. *J Cardiovasc Magn Reson*. 2019;21:1–9.

60. Khalique Z, Ferreira PF, Scott AD, et al. Diffusion tensor cardiovascular magnetic resonance in cardiac amyloidosis. *Circ Cardiovasc Imaging*. 2020;13:e009901.

61. Giblin GT, Cuddy SAM, González-López E, et al. Effect of tafamidis on global longitudinal strain and myocardial work in transthyretin cardiac amyloidosis. *Eur Heart J Cardiovasc Imaging*. 2022;23:1029–1039.

62. Huntjens PR, Zhang KW, Soyama Y, Karmpalioti M, Lenihan DJ, Gorcsan J III. Prognostic utility of echocardiographic atrial and ventricular strain imaging in patients with cardiac amyloidosis. *J Am Coll Cardiol Img*. 2021;14:1508–1519.

63. Clemmensen TS, Eiskjær H, Ladefoged B, et al. Prognostic implications of left ventricular myocardial work indices in cardiac amyloidosis. *Eur Heart J Cardiovasc Imaging*. 2021;22:695–704.

64. Maurer MS, Schwartz JH, Gundapaneni B, et al. Tafamidis treatment for patients with transthyretin amyloid cardiomyopathy. *N Engl J Med*. 2018;379:1007–1016.

65. Milani P, Dispenzieri A, Scott CG, et al. Independent prognostic value of stroke volume index in patients with immunoglobulin light chain amyloidosis. *Circ Cardiovasc Imaging*. 2018;11:e006588.

66. Sperry BW, Vranian MN, Tower-Rader A, et al. Regional variation in technetium pyrophosphate uptake in transthyretin cardiac amyloidosis and impact on mortality. *J Am Coll Cardiol Img*. 2018;11:234–242.

67. Castano A, Haq M, Narotsky DL, et al. Multicenter study of planar technetium 99m pyrophosphate cardiac imaging: predicting survival for patients with ATTR cardiac amyloidosis. *JAMA Cardiol*. 2016;1:880–889.

68. Fontana M, Martinez-Naharro A, Chacko L, et al. Reduction in CMR derived extracellular volume with patisiran indicates cardiac amyloid regression. *J Am Coll Cardiol Img*. 2021;14:189–199.

69. Castaño A, DeLuca A, Weinberg R, et al. Serial scanning with technetium pyrophosphate (99mTc-PYP) in advanced ATTR cardiac amyloidosis. *J Nucl Cardiol*. 2016;23:1355–1363.

70. Hanna M, Ruberg FL, Maurer MS, et al. Cardiac scintigraphy with technetium-99m-

labeled bone-seeking tracers for suspected amyloidosis: JACC review topic of the week. *J Am Coll Cardiol*. 2020;75:2851–2862.

71. Lee SP, Lee ES, Choi H, et al. 11C-Pittsburgh B PET imaging in cardiac amyloidosis. *J Am Coll Cardiol Img*. 2015;8:50–59.

72. Park MA, Padera RF, Belanger A, et al. 18F-Florbetapir binds specifically to myocardial light chain and transthyretin amyloid deposits: autoradiography study. *Circ Cardiovasc Imaging*. 2015;8:e002954.

73. Rosengren S, Skibsted Clemmensen T, Tolbod L, et al. Diagnostic accuracy of [11C] PIB positron emission tomography for detection of cardiac amyloidosis. *J Am Coll Cardiol Img*. 2020;13:1337–1347.

74. Takasone K, Katoh N, Takahashi Y, et al. Non-invasive detection and differentiation of cardiac amyloidosis using ^{99m}Tc-pyrophosphate scintigraphy and 11C-Pittsburgh compound B PET imaging. *Amyloid*. 2020;27:266–274.

75. Robinson AA, Chow K, Salerno M. Myocardial T1 and ECV measurement: underlying concepts and technical considerations. *J Am Coll Cardiol Img*. 2019;12:2332–2344.

76. Rettl R, Mann C, Duca F, et al. Tafamidis treatment delays structural and functional changes of the left ventricle in patients with transthyretin amyloid cardiomyopathy. *Eur Heart J Cardiovasc Imaging*. 2022;23:767–780.

77. Garcia-Pavia P. Aus dem Siepen F, Donal E, et al. Phase 1 trial of antibody NI006 for depletion of cardiac transthyretin amyloid. *N Engl J Med*. 2023;389:239–250.

78. Dorbala S, Park MA, Cuddy S, et al. Absolute quantitation of cardiac (99m)Tc-pyrophosphate using cadmium-zinc-telluride-based SPECT/CT. *J Nucl Med*. 2021;62:716–722.

79. Pilebro B, Arvidsson S, Lindqvist P, et al. Positron emission tomography (PET) utilizing Pittsburgh compound B (PIB) for detection of amyloid heart deposits in hereditary transthyretin amyloidosis (ATTR). *J Nucl Cardiol*. 2018;25:240–248.

80. Dey D, Slomka PJ, Leeson P, et al. artificial intelligence in cardiovascular imaging: JACC state-of-the-art review. *J Am Coll Cardiol*. 2019;73:1317–1335.

81. Jone PN, Gearhart A, Lei H, et al. Artificial intelligence in congenital heart disease. *JACC: Adv*. 2022;1:100153.

82. LeCun Y, Bengio Y, Hinton G. Deep learning. *Nature*. 2015;521:436–444.

83. Chu M, Wu P, Li G, Yang W, Gutiérrez-Chico JL, Tu S. Advances in diagnosis, therapy, and prognosis of coronary artery disease powered by deep learning algorithms. *JACC: Asia*. 2023;3:1–14.

84. Zhang J, Gajjala S, Agrawal P, et al. Fully Automated echocardiogram interpretation in clinical practice. *Circulation*. 2018;138:1623–1635.

85. Huda A, Castaño A, Niyogi A, et al. A machine learning model for identifying patients at risk for wild-type transthyretin amyloid cardiomyopathy. *Nat Commun*. 2021;12:2725.

86. Germain P, Vardazaryan A, Labani A, Padoy N, Roy C, El Ghannudi S. Deep learning to classify AL versus ATTR cardiac amyloidosis MR images. *Biomedicines*. 2023;11(1):193.

87. Delbarre MA, Girardon F, Roquette L, et al. Deep learning on bone scintigraphy to detect abnormal cardiac uptake at risk of cardiac amyloidosis. *J Am Coll Cardiol Img*. 2023;16:1085–1095.

88. Halme HL, Ihalainen T, Suomalainen O, et al. Convolutional neural networks for detection of transthyretin amyloidosis in 2D scintigraphy images. *EJNMMI Res*. 2022;12:27.

89. Goto S, Mahara K, Beussink-Nelson L, et al. Artificial intelligence-enabled fully automated detection of cardiac amyloidosis using electrocardiograms and echocardiograms. *Nat Commun*. 2021;12:2726.

90. Goto S, Solanki D, John JE, et al. Multinational federated learning approach to train ECG and echocardiogram models for hypertrophic cardiomyopathy detection. *Circulation*. 2022;146:755–769.

91. Bonnefous L, Kharoubi M, Bézard M, et al. Assessing cardiac amyloidosis subtypes by unsupervised phenotype clustering analysis. *J Am Coll Cardiol*. 2021;78:2177–2192.

92. Cotella JI, Slivnick JA, Sanderson E, et al. Artificial intelligence based left ventricular ejection fraction and global longitudinal strain in cardiac amyloidosis. *Echocardiography*. 2023;40:188–195.

93. Santarelli MF, Genovesi D, Positano V, et al. Deep-learning-based cardiac amyloidosis classification from early acquired pet images. *Int J Cardiovasc Imaging*. 2021;37:2327–2335.

94. Lo Iacono F, Maragna R, Pontone G, Corino VDA. A robust radiomic-based machine learning approach to detect cardiac amyloidosis using cardiac computed tomography. *Frontn Radiol*. 2023;3:1193046.

95. Satriano A, Afzal Y, Sarim Afzal M, et al. Neural-network-based diagnosis using 3-dimensional myocardial architecture and deformation: demonstration for the differentiation of hypertrophic cardiomyopathy. *Front Cardiovasc Med*. 2020;7:584727.

96. Martini N, Aimo A, Barison A, et al. Deep learning to diagnose cardiac amyloidosis from cardiovascular magnetic resonance. *J Cardiovasc Magn Reson*. 2020;22:84.

97. Agibetov A, Kammerlander A, Duca F, et al. Convolutional neural networks for fully automated diagnosis of cardiac amyloidosis by cardiac magnetic resonance imaging. *J Pers Med*. 2021;11(12):1268.

98. Germain P, Vardazaryan A, Padoy N, et al. Deep learning supplants visual analysis by experienced operators for the diagnosis of cardiac amyloidosis by cine-CMR. *Diagnostics (Basel)*. 2021;12(1):69.

99. Krittanawong C, Johnson KW, Rosenson RS, et al. Deep learning for cardiovascular medicine: a practical primer. *Eur Heart J*. 2019;40:2058–2073.

100. Sengupta PP, Shrestha S, Berthon B, et al. Proposed Requirements for Cardiovascular Imaging-Related Machine Learning Evaluation (PRIME): a checklist: reviewed by the American College of Cardiology Healthcare Innovation Council. *J Am Coll Cardiol Img*. 2020;13:2017–2035.

101. Dey D, Arnaout R, Antani S, et al. Proceedings of the NHLBI workshop on artificial Intelligence in cardiovascular imaging: translation to patient care. *J Am Coll Cardiol Img*. 2023;16(9):1209–1223.

KEY WORDS AI, amyloidosis, cardiac ATTR, cardiac magnetic resonance, CMR, DL, echocardiography, ML, multimodality imaging, scintigraphy, SPECT